Journal of Crystal Growth 353 (2012) 35–38

Contents lists available at SciVerse ScienceDirect

Journal of Crystal Growth

journal homepage: www.elsevier.com/locate/jcrysgro

Effect of surface defects on InGaAs/InAlAs Quantum Cascade mesa current–voltage characteristics

Nyan L. Aung [a,*], Xue Huang [a], Williams O. Charles [a,1], Nan Yao [b], Claire F. Gmachl [a]

[a] Department of Electrical Engineering, Princeton University, Princeton, NJ 08544, USA
[b] The Imaging and Analysis Center, Princeton University, Princeton, NJ 08544, USA

ARTICLE INFO

Article history:
Received 18 March 2012
Received in revised form
24 April 2012
Accepted 26 April 2012
Communicated by K.H. Ploog
Available online 5 May 2012

Keywords:
A3. Molecular beam epitaxy
A3. Quantum wells
B2. Semiconducting III–V materials
B3. Quantum Cascade device

ABSTRACT

We investigate the impact of surface defect density on the transport properties of molecular beam epitaxy grown InGaAs/AlInAs Quantum Cascade (QC) structures. We examine six parameters of the current–voltage (*IV*) characteristics of the QC mesas: turn-on voltage, turn-on current density, turn-on differential resistance, differential resistance, cut-off voltage, and cut-off current density. The analyses for pulsed mode operation ($T=80$ K and 300 K) and continuous wave (CW) operation (80 K) show that all six parameters are only weakly correlated to surface defects. The turn-on voltage and current density share a negative correlation with defects (>-0.26) in both pulsed mode and CW operation at 80 K, and a positive correlation in pulsed mode at 300 K (<0.21). The cut-off voltage has a positive correlation in all three modes of operation (<0.51). The cut-off current density has a positive correlation (<0.39) in both pulsed mode (80 K and 300 K) and a negligible correlation in CW operation (80 K). We observed insignificant correlation coefficients (<0.1) for differential resistances at 80 K along with a weak negative correlation (>-0.29) in pulsed mode at 300 K. Our analysis demonstrates that shallow oval and a few deep oval defects have little influence on *IV*.

1. Introduction

Quantum Cascade (QC) lasers are promising mid-infrared light sources for gas sensing, free-space communication, and medical diagnostics due to their small size, high performance at room temperature, and the possibility to tailor their emission wavelength. QC lasers are typically fabricated using InP- or GaAs-based III–V semiconductor quantum well heterostructures. State-of-the-art performance QC lasers can be grown by either molecular beam epitaxy (MBE) or metal organic chemical vapor deposition (MOCVD). It is well known that MBE-grown GaAs and related heterostructures can contain a large number of macroscopic defects, so called oval defects, with sizes ranging from a few to several tens of microns and the surface density varying from 10^2 to 10^5 cm^{-2} [1–4]. Studies on threading dislocation and oval defects have revealed that defects influence the electrical property of the device [5–7]. However, the effect of defects on electrical properties of QC devices is still unknown. The performance variation of QC devices fabricated on a given wafer can be due to the inherent property of QC structure and the non-inherent properties such as defects. Thus, it is necessary to examine how much defects influence the performance of QC device. Here, we describe the dislocation and surface defects observed in an InGaAs/AlInAs QC structure grown by MBE and the effect of macroscopic surface defects on current–voltage (*IV*) characteristics.

2. QC structure and characterization of defects

The MBE grown QC structure studied here has $In_{0.52}Al_{0.48}As$ and $In_{0.53}Ga_{0.47}As$ lattice matched to a low doped ($n\sim1\times10^{17}$ cm^{-3}) InP substrate. It has the same active core structure reported in Ref. 8.The Si doping is 3×10^{17} cm^{-3}, instead of 1.5×10^{17} cm^{-3} in the same layers in the injector region. The structure consists of 55 stages of repeated alternating active and injector regions, inserted between a 0.6 μm thick $In_{0.53}Ga_{0.47}As$ lower waveguide layer (doped $n\sim6\times10^{16}$ cm^{-3}) and a 2 μm thick $In_{0.53}Ga_{0.47}As$ upper waveguide layer (doped $n\sim6\times10^{16}$ cm^{-3}). The upper waveguide is followed by a 0.6 μm thick $In_{0.53}Ga_{0.47}As$ plasmon layer (doped $n\sim5\times10^{18}$ cm^{-3}) and a 0.05 μm thick $In_{0.53}Ga_{0.47}As$ contact layer (doped $n\sim2\times10^{19}$ cm^{-3}).

To examine the dislocation in a QC structure, a Philips CM200 FEG-TEM transmission electron microscope is used. The samples are prepared by cleaving, polishing, cutting with ultrasonic disk cutter, embedding into metal tube, thinning down to about 100 μm and finally ion milling. A dislocation observed in a

* Corresponding author. Tel.: +1 207 376 7669.
E-mail address: naung@princeton.edu (N.L. Aung).
[1] Current address: Phononic Devices, Inc., 1730 Varsity Drive, Ste 220, Raleigh, NC 27606, USA.

0022-0248/$ - see front matter © 2012 Elsevier B.V. All rights reserved.
http://dx.doi.org/10.1016/j.jcrysgro.2012.04.037

QC structure is shown in Fig. 1. The dislocation runs through multiple periods of active and injector regions. In the region about 25 nm wide along the misfit plane, the thickness and the direction of QC layers change, indicating that the dislocation adversely affects the desired QC structure. The dislocation in Fig. 1 is tilted about 60° to the normal surface of epilayers and runs through the active core. We estimate that the distorted region due to a single dislocation line can occupy up to 0.06% of a 190 μm diameter round mesa.

We observed two types of macroscopic surface defects. Deep defects are highly visible while shallow defects are seen as surface roughness (Fig. 2(a)). The typical size distribution of both defects is presented in Fig. 3. The number of deep defects is 0–8 per device while the number of shallow defects can be up to 36 per device. In order to inspect the cross-sectional view of a representative macroscopic surface defect, a FEI Strata TM DB 235 focused ion beam (FIB) milling tool was used to drill the wedge holes. Scanning electron microscope (SEM) images of the cross-sectional surface walls are taken by a high performance Quanta 200 FEG ESEM. As shown in Fig. 2(b), a cavity beneath the deep defect implies that the defect originates at the QC active core. This kind of cavity is not observed for the shallow defect (Fig. 2(c)). The SEM image indicates that the shallow defects originate only near the surface. This wafer was processed into round mesas with 190 μm diameters and 10 μm height. In order to record the defect density, each mesa is photographed using an optical microscope.

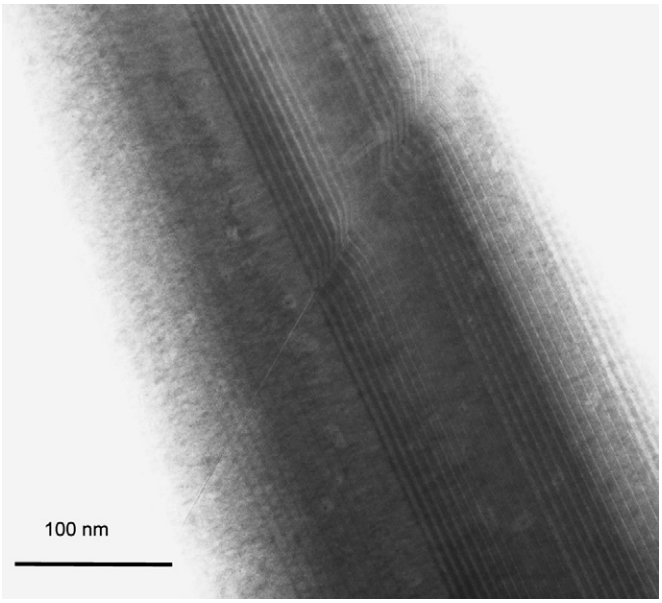

Fig. 1. TEM image of dislocation in quantum cascade structure.

In QC lasers, electrons from the injector regions are transported into the active regions by phonon-assisted scattering and resonant tunneling between the injector ground level and the upper laser level. There, they make radiative transitions from upper to lower laser states, and eventually enter the next injector regions. The efficient electron transport into the active region is an important mechanism governing QC laser performance benchmarks, such as wall plug efficiency [9]. The electron transport properties can be inferred from *IV* curves. To determine how *IV* curves vary with the number of defects, six parameters in the *IV* curves are studied as illustrated in Fig. 4. Turn-on voltage, turn-on current density, cut-off voltage, and cut-off current density are calculated from the highest curvature points within certain regions of interest on the *IV* curves. Turn-on voltage is the voltage required to enable electron transport [10]. As the applied voltage keeps increasing, the QC device eventually encounters the cut-off voltage at which the ground state in the injector is no longer aligned with the upper laser state, forming a kink in the *IV*. Eventually, the ground state in the injector aligns with higher states above the upper laser state and the current flows again. Turn-on and cut-off current densities are physical parameters corresponding to the above two voltages. Differential resistances before and after turn-on voltage are computed from linearly fitting the slope of *IV* curves in the corresponding regions. The current flow through the device before the turn-on voltage is negligible. Once the applied voltage is above the turn-on voltage, the device becomes highly conductive. In this region, differential resistance originates mainly from the waveguide layers and the active region where resistivity is mainly governed by tunneling and the scattering time.

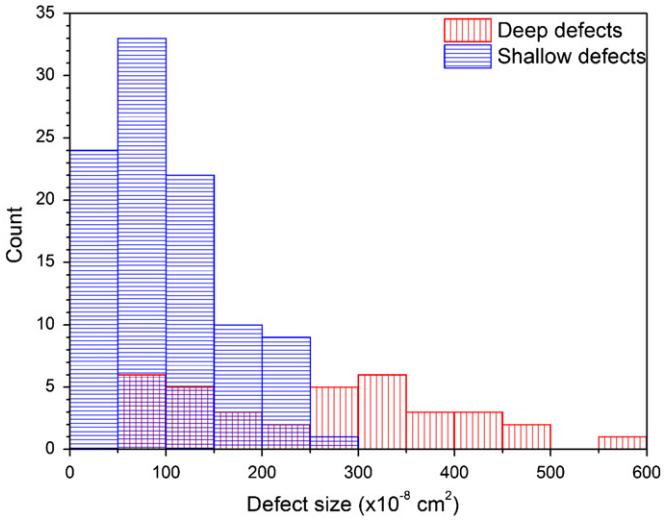

Fig. 3. Defect size distribution taken from 10 representative mesas.

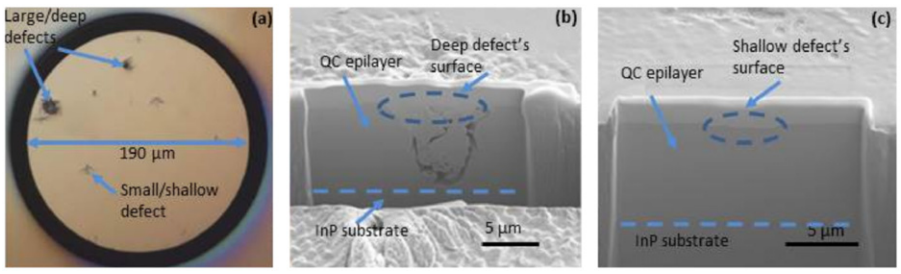

Fig. 2. Optical microscope image (top view) of a mesa with two types of defects (a). SEM image of the cross-sectional view of a large/deep defect (b) and a shallow defect (c).

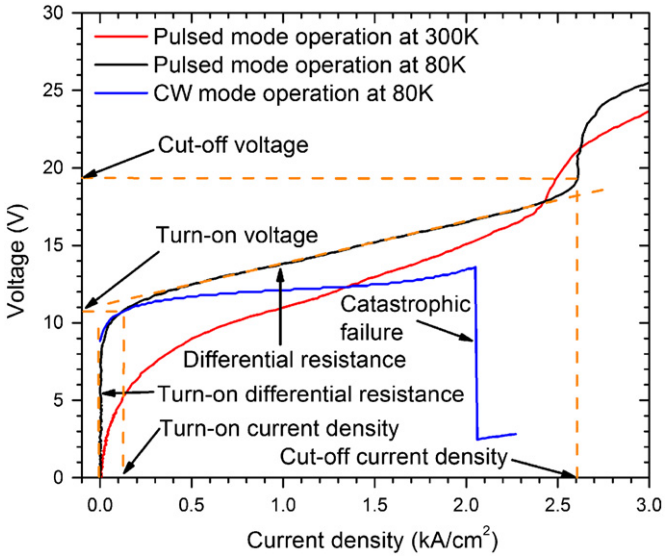

Fig. 4. Typical *IV* curves of a 190 μm diameter mesa with quantum cascade structure at three modes of operations and the six parameters systematically investigated. In continuous wave (CW) operation, the device eventually broke down at a certain voltage.

3. Results and discussion

We performed forward bias experiments on pulsed mode operation at both 80 K and 300 K heat sink temperatures and continuous wave (CW) operation at 80 K. The experimental result on pulsed mode operation at 80 K is shown in Fig. 5 and a summary of the analysis is presented in Table 1. While the turn-on voltage slightly decreases with increasing number of defects, the turn-on current density decreases considerably.

Table 1
Summary of experiments with pulsed mode operation (T=80 K).

Parameters	Linear slope	Mean values	Correlation coefficient
Turn-on voltage	−0.008 V/defect	10.8 V	−0.22
Turn-on current dsensity	−1 A/cm^2 defect	130 A/cm^2	−0.26
Turn-on differential resistance	10 Ω/defect	4943 Ω	0.043
Differential resistance	0.0004 Ω/defect	8.6 Ω	0.005
Cut-off voltage	0.05 V/defect	19.5 V	0.51
Cut-off current density	8 A/cm^2 defect	2820 A/cm^2	0.39

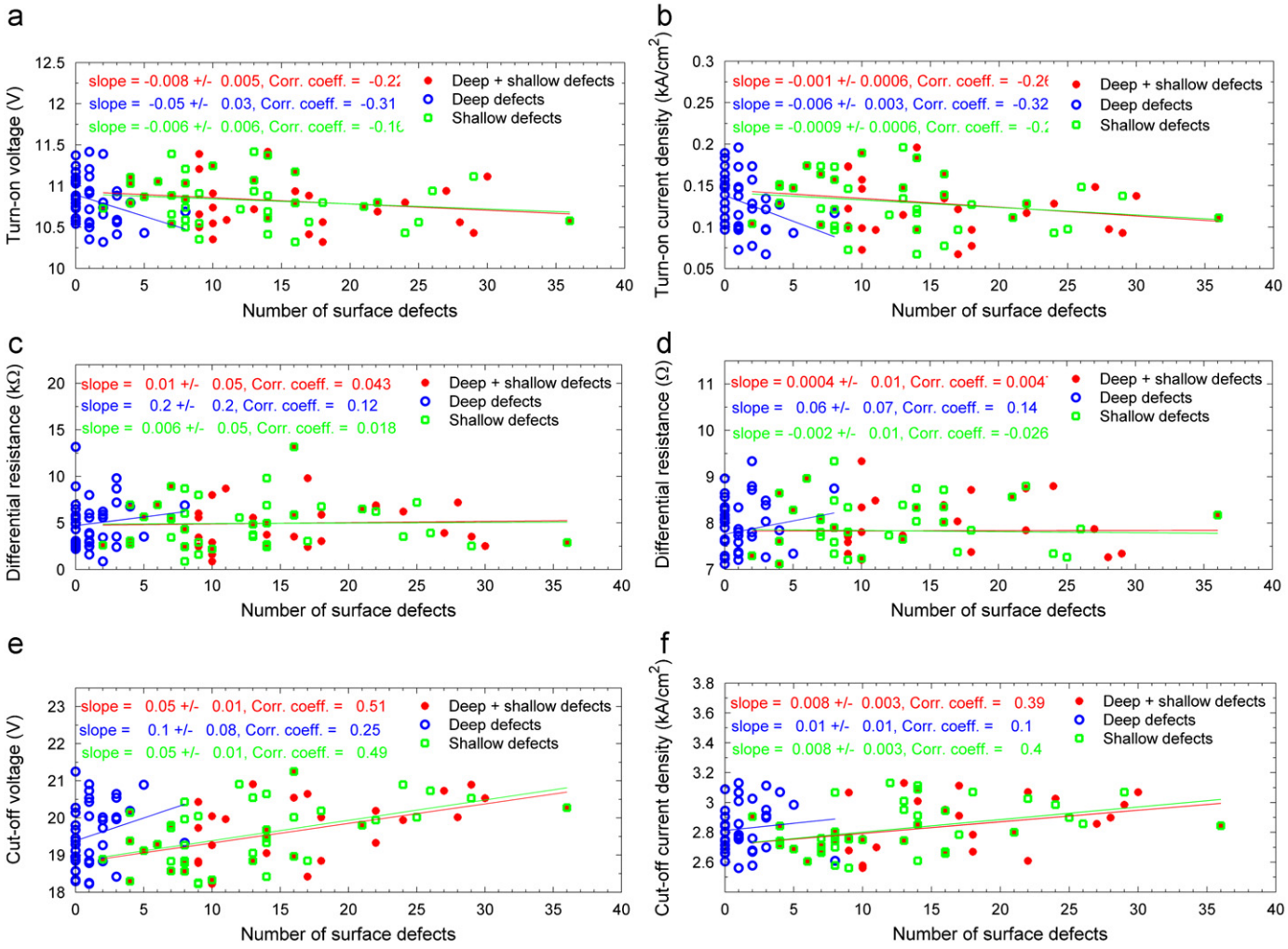

Fig. 5. Experimental results for devices operated in pulsed mode at 80 K describing the correlation between surface defects and turn-on voltage (a), turn-on current density (b), turn-on differential resistance (c), differential resistance (d), cut-off voltage (e), and cut-off current density (f).

Table 2
Summary of experiments with pulsed mode operation ($T=300$ K).

Parameters	Linear slope	Mean values	Correlation coefficient
Turn-on voltage	0.005 V/defect	9.9 V	0.18
Turn-on current density	2 A/cm^2 defect	680 A/cm^2	0.21
Turn-on differential resistance	−0.2 Ω/defect	101 Ω	−0.2
Differential Resistance	−0.03 Ω/defect	13 Ω	−0.29
Cut-off voltage	0.01 V/defect	17.6 V	0.25
Cut-off current density	5 A/cm^2 defect	2530 A/cm^2	0.29

Table 3
Summary of experiments with CW mode operation ($T=80$ K).

Parameters	Linear slope	Mean values	Correlation coefficient
Turn-on voltage	−0.007 V/defect	11.7 V	−0.23
Turn-on current density	−2 A/cm^2 defect	570 A/cm^2	−0.17
Differential resistance	−0.009 Ω/defect	2 Ω	−0.036
Cut-off voltage	0.02 V/defect	11.8 V	0.2
Cut-off current density	−3 A/cm^2 defect	1760 A/cm^2	−0.064

When the number of defects is increased by 20, the turn-on voltage and current density decrease by 1.5% and 15.4% respectively with data variation of 10.1% and 98.9%. The negligible correlation coefficients (<0.1) for differential resistances indicate that defects are not the cause of resistance variation. The turn-on differential resistance varies by 249% and the differential resistance has a variation of 26%. However, the cut-off voltage and current density share a moderate positive correlation (0.51 and 0.39 respectively) with the number of defects. For an increase in 20 defects, the cut-off voltage and current density increase by 5% and 4.3% respectively while data variations of these are 15.5% and 20.2% respectively. The turn-on current density and turn-on differential resistance have large spreads in data due to the fluctuations in the low current regime.

Table 2 shows a summary of the analysis for room temperature pulsed mode operation (see also Supplementary information, Fig. S1). The correlations between all six parameters and defects are low (correlation coefficient magnitude <0.3). Adding 20 defects will cause the turn-on voltage and the turn-on current density to rise by 1% and 5.9%, the turn-on differential resistance and the differential resistance to drop by 4% and 4.6%, and the cut-off voltage and the cut-off current density to surge by 1.1% and 4% respectively. The changes are smaller than 9.9%, 46.2%, 31%, 22.5%, 10.7% and 23% data variations of the turn-on voltage, the turn-on current density, the turn-on differential resistance, the differential resistance, the cut-off voltage, and the cut-off current respectively. These large data variations are of concern.

Finally, CW operation at 80 K is performed on a different set of mesas and a summary of the analysis is presented in Table 3 (see Supplementary information, Fig. S2). In CW measurement, 28% of the mesas failed, but we did not detect any dependence of device failure on both types of surface defects. Due to the limitation of the CW power source, we could not reliably determine the turn-on differential resistance. Again, the correlations between all five parameters and defects are low (correlation coefficient magnitude <0.3). The differential resistance and the cut-off current density have no dependency on defects. Meanwhile, for a 20 defect increase, the turn-on voltage and the turn-on current density decrease by 1.2% and 7%, and the cut-off voltage increases by 3.4% compared with a 3.5%, 27.8% and 10% variations in respective parameters.

Data variation in our measurement comes from computational uncertainty introduced by the measurement noise and the gold wire length disparity. From our analysis, it is clear that defects' influence on *IV* is much smaller than the data variation from intrinsic or spurious sources. It is because the deep defects occupy a tiny fraction of a device's total volume (five deep defects, each with 14 μm diameter, will be only 2.7% of device volume) while shallow defects do not provide any contribution to the *IV* because they do not originate in the active core as shown by the SEM image. However, due to their places of origin, it can be concluded that these defects will scatter the light generated in the device.

4. Conclusion

A TEM image of dislocation and the cross-sectional SEM images of macroscopic surface defects in InGaAs/AlInAs QC structure grown by MBE are presented. *IV* curves of mesas with different numbers of defects are characterized and six parameters on the *IV* curves are analyzed. Our data establish that surface defects have little effect on the electrical properties of QC lasers.

Acknowledgment

The authors would like to acknowledge Gerald R. Poirier and Dr. Shiyou Xu from the Princeton Imaging and Analysis Center for their help in using the FIB and SEM tools. This work is supported in part by MIRTHE (NSF-ERC # EEC-0540832), NSF Grant # ECCS-1028364, NSF Grant # HRD-0833180, NSF Grant # IIP-0917956, and NSF-MRSEC Program through the Princeton Center for Complex Materials (DMR-0819860).

Appendix A. Supporting information

Supplementary data associated with this article can be found in the online version at doi:10.1016/j.jcrysgro.2012.04.037.

References

[1] C.E. Wood, L. Rathbun, H. Ohno, D. Desimone, On the origin and elimination of macroscopic defects in MBE films, Journal of Crystal Growth 51 (1981) 299–303.
[2] K. Fujiwara, K. Kanomoto, Y.N. Ohta, Y. Tokuda, T. Nakayama, Classification and origins of GaAs oval defects grown by molecular beam epitaxy, Journal of Crystal Growth 80 (1987) 104–112.
[3] K. Nanbu, J. Saito, T. Ishikawa, K. Kondo, A. Shibotomi, Classification of surface defects on GaAs grown by molecular beam epitaxy, Journal of the Electrochemical Society 133 (1986) 601–604.
[4] N. Chand, S.N.G. Chu, A comprehensive study and methods of elimination of oval defects in MBE-GaAs, Journal of Crystal Growth 104 (1990) 485–497.
[5] M. Shinohara, T. Ito, K. Wada, Y. Imamura, Electrical properties of oval defects in GaAs grown by MBE, Japanese Journal of Applied Physics 23 (1984) L371–L373.
[6] T. Nakamura, K. Nanbu, T. Ishikawa, K. Kondo, Influence of surface defects on the characteristics of high electron mobility transistors grown by molecular beam epitaxy, Journal of Applied Physics 64 (1988) 2164–2167.
[7] A.R. Arehart, B. Moran, J.S. Speck, U.K. Mishra, S.P. DenBaars, S.A. Ringel, Effect of threading dislocation density on Ni/n-GaN Schottky diode I–V characteristics, Journal of Applied Physics 100 (2006) 023709.
[8] X. Huang, W. Charles, C. Gmachl, Temperature-insensitive long-wavelength ($\lambda=14$ μm) Quantum Cascade lasers with low threshold, Optics Express 19 (2011) 8297–8302.
[9] P.Q. Liu, A.J. Hoffman, M.D. Escarra, K.J. Franz, J.B. Khurgin., Y. Dikmelik, X. Wang, J.Y. Fan, C.F. Gmachl, Highly power-efficient quantum cascade lasers, Nature Photonics 4 (2010) 95–98.
[10] C. Gmachl, F. Capasso, A. Tredicucci, D.L. Sivco, R. Kohler, A.L. Hutchinson, A.Y. Cho, Dependence of the device performance on the number of stages in Quantum-Cascade lasers, IEEE Journal of Selected Topics in Quantum Electronics 5 (1999) 808–816.